Embedded Micro / Nano Channels Formation for Three-Dimensional Negative-Tone Photoresist Microstructuring

Sang-Kon Kim*, Hye-Keun Oh, Young-Dae Jung, and Ilsin An
Department of Applied Physics, Hanyang University, Ansan 426-791, South Korea
*E-mail: sangkona@hotmail.com, *Web: www.sangkon.info

ABSTRACT

Photoresist lithography has been applied in MEMS (micro electro mechanical systems). The flexible 3D (three dimensional) micro / nano fabrication technique and its process simulation tool have required for 3-D MEMS. This paper presents a UV lithography process simulation for the embedded micro / nano channel formation in a negative-tone photoresist. For its purpose, the moving-mask technology and lithography processes of the negative-tone chemically amplified photoresist are modeled. The simulation algorithm of nano-lithography is applied for micro-lithography. The validity of simulation for the proposed 3D microstructuring is successfully confirmed by the comparison between experimental results and simulated results. Hence, the developed modeling and simulation can discuss and optimize photoresist characteristics and lithography process conditions due to the various pattern formations of micro / nano channels.

Keywords: lithography, lithography simulation, negative resist, chemically amplified resist, multi-exposures, inverse lithography, embedded channel, MEMS

1. INTRODUCTION

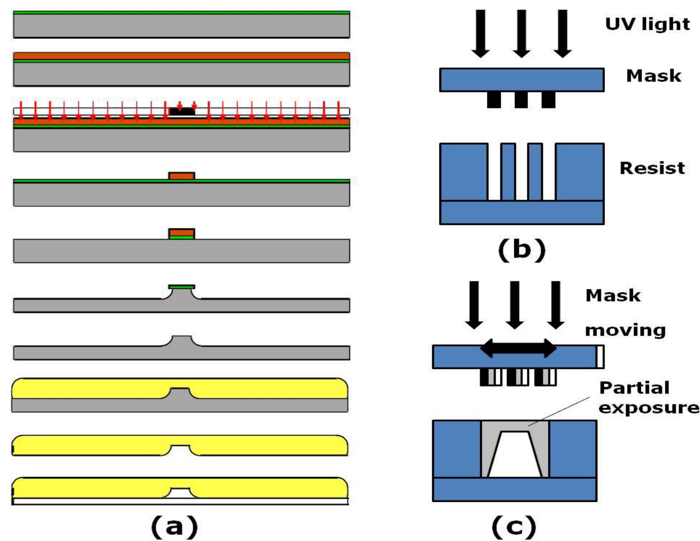

Fig. 1. Schematic drawing of (a) a multi-steps method and (c) the moving-mask lithography for the manufacturing of embedded micro/nano channels, and (b) the normal lithography for the formation of line and space patterns.

The micro / nano systems can manipulate information with light and diagnose the body from the inside, or assemble parts of operating individual atoms and molecules by integrating functional elements in different domains such as mechanics, electronics, chemistry, optics and biotechnology. Application of 3D (three dimensional) photoresist microstructures on a substrate surface has been of great interest, because these microstructures are applicable to various

Advances in Resist Materials and Processing Technology XXVI, edited by Clifford L. Henderson,
Proc. of SPIE Vol. 7273, 72730R · © 2009 SPIE · CCC code: 0277-786X/09/$18 · doi: 10.1117/12.814244

MEMS (micro electro mechanical systems) devices. Although the multi-steps fabrication of micro / nano channels is more complicate and expensive, the moving-mask ultraviolet (UV) lithography can realize micro / nano channels with semi-arbitrary cross-sectional shape with only single exposure step. Figure 1 shows the comparison of the multi-steps method with the moving-mask lithography for the fabrication of embedded micro / nano channels. The multi-steps method are composed of lithography, etch, and coating. Hence, it is more complicate and expensive than the moving-mask lithography. For this novel fabrication method, the lithography process simulation is required to develop and verify process conditions in the thick and thin photoresists. The fast marching method, which calculates the resultant photoresist profile change with development time, was published [1]. In this paper, the embedded micro / nano channels, which are fabricated by the moving-mask UV lithography for a negative chemically amplified resist (CAR), are modeled and simulated by full lithography processes, which are exposure, post exposure process (PEB), and development.

2. MOVING MASK LITHOGRAPHY

For the moving-mask lithography, the deposited dose profile at the part of microchannels' sidewall and ceiling depends on a line and space (L/S) mask pattern under varying the mask-movement trajectory. The sidewall angle increases with the longer mask-movement range. It is expected that optimization of photoresist characteristics and lithography process conditions enable to fabricate the various embedded microchannels.

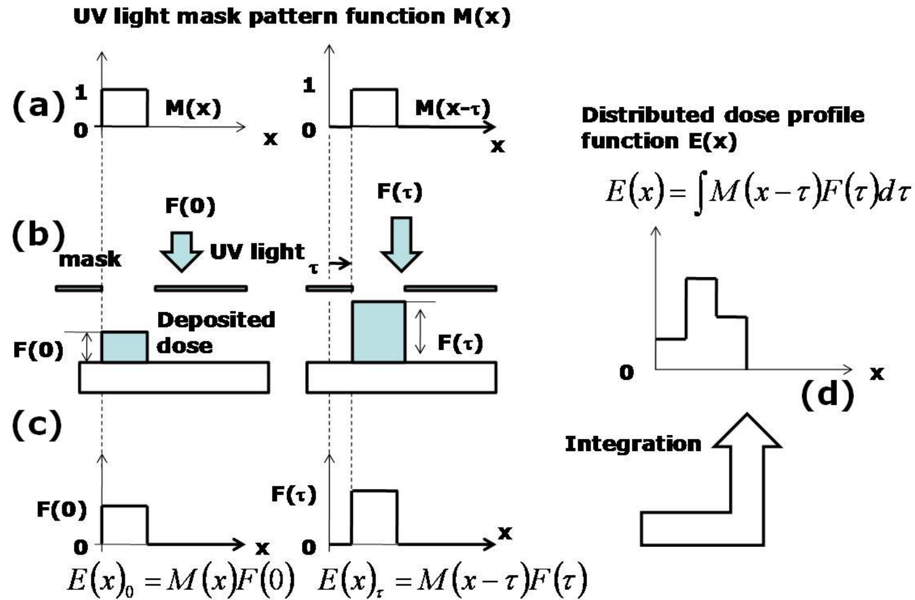

Fig. 2. Exposure step of moving-mask lithography: (a) mask moving, (b) deposited dose at the position where the mask is moved by distance τ, and (c) deposited does on the resist surface at position x, and (d) integrated distributed dose profile deposited over the resist surface [2].

When the mask is moved by distance τ in Fig. 2, the function E(x) of the deposited does on the resist surface at position x is

$$E(x)_\tau = M(x-\tau)F(\tau) \rightarrow E(x) = \int M(x-\tau)F(\tau)d\tau . \quad (1)$$

where $E(x)_\tau$ denotes the deposited dose on the resist surface when the mask is positioned at $x=\tau$ and $F(\tau)$ is a function of the deposited dose at the position where the mask is moved by distance τ. By applying Fourier transformation of Eq. (1), E(x), M(x), and $F(\tau)$ are transformed to E(f), M(f), and F(f) by using the convolution theorem:

$$E(f) = M(f)F(f) \rightarrow F(f) = E(f)/M(f) . \quad (2)$$

By applying the inverse Fourier transformation to Eq. (2), the mask movement pattern function F(τ) is derived. This concept makes it possible to derive the mask movement pattern mathematically which realizes the distributed dose profile corresponding to the target shape without trial and error.

3. NEGATIVE LITHOGRAPHY SIMULATION

The chemically amplified negative-type resists generally contain components, which are a polymer and a photo / radio-sensitive compound called photo acid generator (PAG), and cross-linker. When a negative CAR is irradiated by a deep-ultra violet (DUV), the PAG generates acid, and the acid catalyzes cross-linking reactions among the polymer chains directly or through the cross-linker during PEB. The cross-linking leads to the formation of polymer clusters and finally to a gel state, which is considered insoluble to the developer. The developer dissolves single and uncross-linked polymer chains. As a result, the region of the resist film with the absorbed radiation becomes less soluble than the neighboring regions with non-absorbed radiation. The neighboring regions dissolve faster and reveal the surface of the substrate.

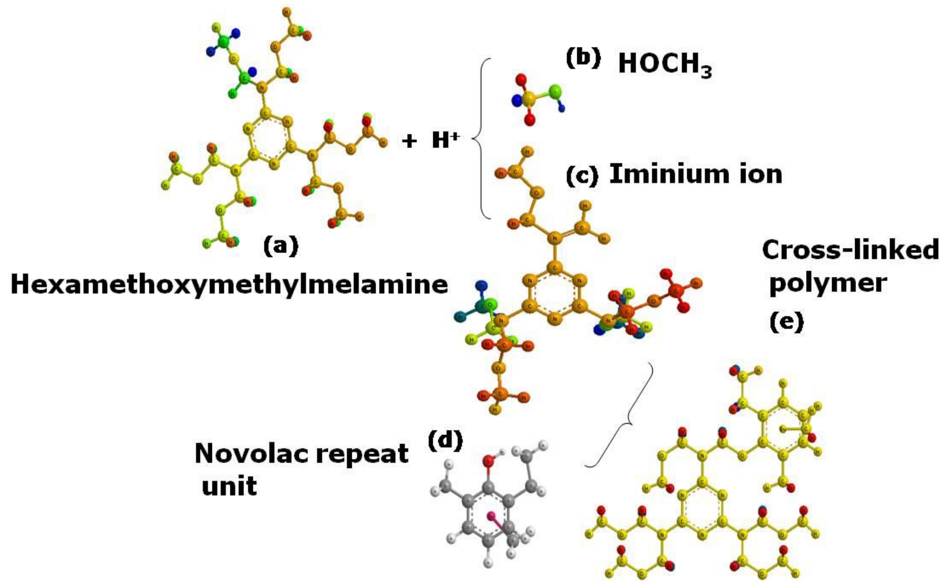

Fig. 3. Cross-linking mechanism for SAL 605 during PEB: (a) Hexamethoxymethylmelamine, (b) $HOCH_3$, (c) iminium ion, (d) novolac repeat unit, and (e) cross-linked polymer.

Figure 3 shows the cross-linking mechanism for a commercial negative-tone CAR, SAL 605, during PEB by using the ChemOffice of CambridgeSoft Ins. A photogenerated Bronsted acid must first encounter a lone pair on one of the oxygens of hexamethoxymethylmelamin (HMM), and cleavage occurs to produce methanol. These result in the creation of an iminium ion. A bimolecular reaction occurs between the iminium ion and a novolac [3]. The cross-linking reaction caused by the photon energy generated in the exposure process is

$$\frac{d[S_{ci}]}{dt} = -k_{photo} \bullet [S_{ci}] \bullet I , \tag{3}$$

where t is the exposure time, k_{photo} is the cross-linking reaction constant for the cross-linking reaction attributable to the photon energy generated by exposure, I is the illumination of exposure light, and S_{ci} is the normalized concentration of the reactive groups in the cross-linking agent. For CAR, exposing the resist to DUV light generates acid from the PAG.

$$\frac{d[PAG]}{dt} = -C \bullet [PAG] \bullet I , \tag{4}$$

$$[H^+]_t = [PAG]_{t=0} - [PAG]_t = [PAG]_{t=o}\left(1 - e^{-CE}\right), \tag{5}$$

where *PAG* is photo-acid generator, *E* is exposure dose, and *C* is a Dill's parameter [4]. During PEB, the photo-generated acid catalyzes a thermally induced reaction:

$$\frac{d[H^+]}{dt'} = -k_{loss} \bullet [H^+] + \nabla \bullet \left(D_{acid} \nabla [H^+]\right) \ , \tag{6}$$

$$\frac{d[S_{ci}]}{dt'} = -k_{ci} \bullet [H^+]^m \bullet [S_{ci}] \ , \tag{7}$$

where t' is the PEB time (sec), $[H^+]^m$ is the acid concentration, D_{acid} $(= k_{0acid} \exp(-E_{aacid}/RT))$ is the diffusion constant of the acid, *m* is the order of the cross-linking reaction, k_{ci} $(= k_{0ci} \exp(-E_{aci}/RT))$ is the cross-linking reaction constant, k_{loss} $(= k_{0loss} \exp(-E_{aloss}/RT))$ is the constant corresponding to the deactivation of the acid in the PEB, and E_{aacid}, E_{aci}, and E_{aloss} indicate the activation energies.

4. SIMULATION AND ANALYSIS

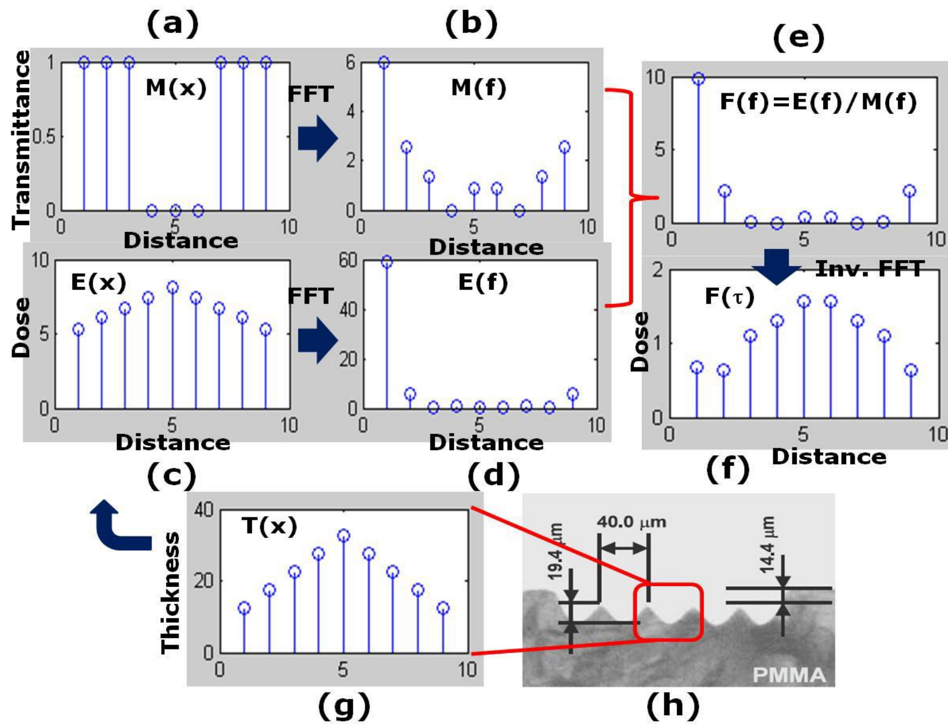

Fig. 4. Calculation method of the distributed dose profile deposited over the resist surface for a positive-tone resist: (a) mask function M(x), (b) Fourier transformation M(f) of M(x), (c) deposited does E(x) on the resist surface at position x, (d) Fourier transformation E(f) of E(x), (e) Fourier transformation F(f), (f) distributed dose F(τ) over the mask according to the position where the mask is moved by distance τ, (g) target shape function T(x), and (h) cross-section of the fabricated microstructure [2]. 'FFT' in the graph legends between (a) and (b) indicates 'Fast Fourier Transformation'. 'Inv. FFT' in the graph legends between (e) and (f) indicates 'Inverse Fast Fourier Transformation'.

Figure 4 show the distributed dose profile deposited over the positive-tone resist surface. A possible factor, which the Inverse approach requires the correction to yield the successful results, is conversion step from the target shape function T(x) to the distributed dose profile function E(x). The dependence of the processed depth on the deposited dose previously obtained through the normal exposure without the mask movement under a fixed development time is applied to the convection. The inverse approach provides derivations of not only the suitable mask movement pattern but also the optimal mask, which contributes to reduce the time and cost for prototyping [5].

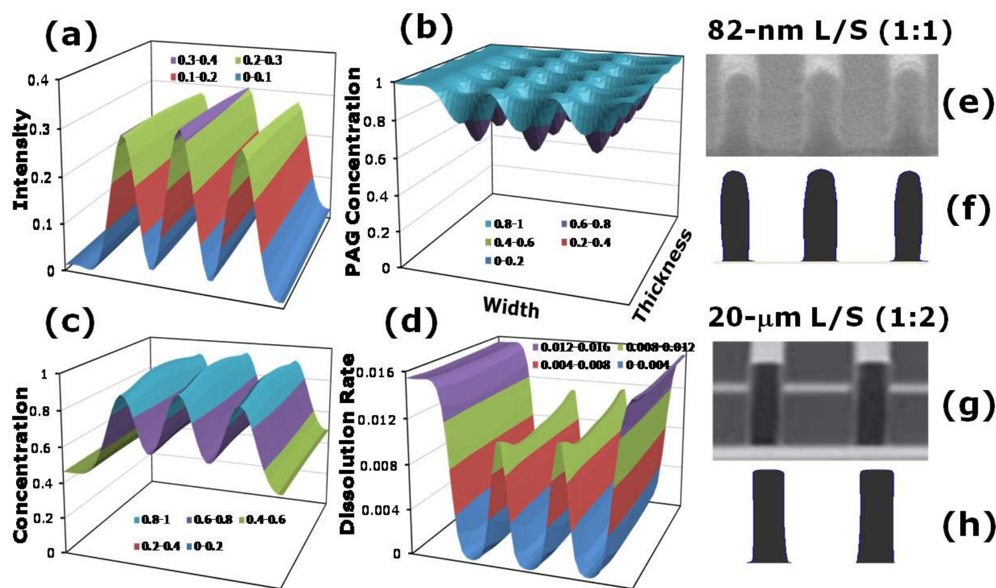

Fig. 5. Simulation results of negative CAR processes: (a) aerial image, (b) PAG concentration, (c) cross-linked polymer concentration, (d) development rate concentration, (e) and (g) experimental results [6, 7], and (f) and (h) simulation results for a 82-nm line and space (L/S = 1:1) pattern and a 20-μm (L/S = 1:2) pattern, respectively.

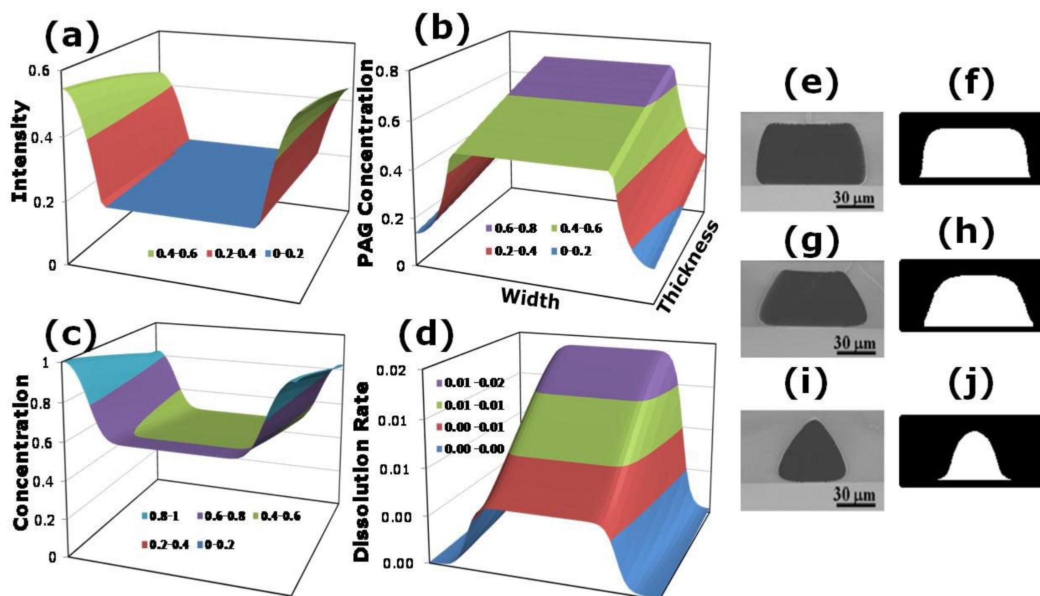

Fig. 6. Simulation results of negative CAR processes for embedded micro channels: (a) aerial image, (b) PAG concentration, (c) cross-linked polymer concentration, (d) development rate concentration, (e), (g), and (i) experimental results [1], and (f), (h), and (j) simulation results.

Figures 5 (a)-(d) and (f) show simulation results of negative CAR processes for a 82-nm line and space (L/S) pattern formation. Simulation results of a negative CAR are aerial image, PAG concentration after exposure process, cross-linked polymer concentration after PEB corresponding to de-protected inhibitor concentration in a positive resist,

dissolution rate concentration for development, and pattern profile. Simulation results in Figs. 5 (f) and (h) are good agreements with experiment results in Figs. 5 (e) and (g). For a 82-nm (L/S = 1:1) pattern formations in Figs. 5 (e) and (f), both experiment conditions and simulation conditions are 193-nm wavelength, a resist of 90-nm ARC thickness and 210-nm resist thickness, 6 % attenuated phase-shifting mask, 0.75 NA, annular illumination with outer 0.89 σ and inner 0.55 σ, 25.6 mJ/cm^2 exposure, post-apply bake (PAB) at 105 °C with 60 sec, PEB at 105 °C for 60 sec, and development for 60 sec [6]. For a 20-μm (L/S = 1:2) pattern formation, both experiment conditions and simulation conditions are 365-nm wavelength, 90-nm ARC thickness, 74-μm resist thickness, 0.63 NA, convention illumination with 0.6 σ, 150 mJ/cm^2 exposure, 1st-PAB at 65 °C with 2 minutes, 2nd-PAB at 95 °C with 6 minutes, 1st-PEB at 65 °C with 2 minutes, 2nd-PEB at 95 °C with 6 minutes, and development for 10 minutes [7].

Figure 6 (a)-(d) and (f) show simulation results of the embedded micro channels due to the dependence of cross-sectional shapes on the mask-movement trajectory. Simulation results of a negative CAR are aerial image, PAG concentration after exposure process, cross-linked polymer concentration after PEB corresponding to the de-protected inhibitor concentration in a positive resist, dissolution rate concentration for development, and pattern profile, respectively. Aerial image of the normal lithography in Fig. 1 (b) are modified into the deposited does of mask-moving lithography on the resist surface by using Inverse approach, which is conversion step from the target shape function in Fig. 4 (g). Various channel shapes correspond to various aerial images. Simulation results in Figs. 6 (f), (h), and (j) are good agreement with experiment results in Figs. 6 (e), (g), and (i). Both experiment conditions and simulation conditions are 100-μm pattern width, 1-μm space width, and 150 mJ/cm^2 incident dose, 50-μm resist thickness, 1st-PEB at 65 °C with 1 minute, 2nd-PEB at 95 °C with 4 minutes, and development for 8 minutes [6]. Simulation of the embedded nano channels can be possible in terms of the simulation results of the nano L / S pattern in Fig. 5.

5. CONCLUSION

The moving-mask lithography concept can serve as a high precise 3D micro / nano fabrication method, because 3D photoresist microstructure can be defined by the moving mask trajectory. For the various 3D micro / nano channel formations in thick / thin photoresists, the post-exposure bake process of a chemically amplified negative-tone resist is modelled by a new modeling method with cross-linking and diffusing process. For the confidence of modeling and simulation, thick / thin line and space patterns and various shape embedded channels are compared with those of experiment. Simulated results are good matching to experimental results. Its accomplishment and improvement can yield not only an effective way to minimize time and cost for 3D microstructuring, but also a basic study of both optics and resist materials.

REFERENCES

[1] Y. Hirai, Y. Inamoto, K. Sugano, T. Tsuchiya, and O. Tabata, "Moving mask UV lithography for three-dimensional structuring," J. Micromech. Microeng. **17**, 199-206 (2007).

[2] N. Matsuzuka and O. Tabata, "Algorithm to derive optimal mask and movement patterns in moving mask deep X-ray lithography (M2DXL)," IEEJ Trans. SM, **125**, 5, 222-228, (2005).

[3] G. P. Patsis and N. Glezos, "Theoretical discussion of diffusion effects in negative chemically amplified resists based on contrast curve simulation," J. Vac. Sci. Technol. B **20**(4), 1303 (2002).

[4] S.-K. Kim, "Thermal effects study of chemically amplified resist," Proc. SPIE **6153**, 61533R (2006).

[5] S.-K. Kim, "Double patterning study with inverse lithography," Proc. SPIE **6923**, 692323 (2008).

[6] K. Patel, M. Lawson, P. Varanasia, D. Medeirosb, G. Wallraff, P. Brock, R. DiPietroc, Y. Nishimura, T. Chibad, and M. Slezake, "IBM-JSR 193nm negative tone resist: polymer design, material properties, and lithographic performance," Proc. SPIE **5376**, 536874 (2004).

[7] Y. Sensu, A. Sekiguchi, S. Mori, and N. Honda, "Profile simulation of SU-8 thick film resist," Proc. SPIE **5753**, 1170 (2005).